

Observational evidence of the accelerated expansion of the universe

Pierre Astier and Reynald Pain

Laboratoire de Physique Nucléaire et de Hautes Energies, Université Pierre et Marie Curie, Université Paris Diderot and CNRS/IN2P3, 4 place Jussieu, 75005 Paris, France

Abstract

The discovery of cosmic acceleration is one of the most important developments in modern cosmology. The observation, thirteen years ago, that type Ia supernovae appear dimmer than they would have been in a decelerating universe followed by a series of independent observations involving galaxies and clusters of galaxies as well as the cosmic microwave background, all point in the same direction: we seem to be living in a flat universe whose expansion is currently undergoing an acceleration phase. In this paper, we review the various observational evidences, most of them gathered in the last decade, and the improvements expected from projects currently collecting data or in preparation.

1 Introduction

Soon after the expansion of the universe was firmly established, were observational cosmologists already trying to detect a modification of the expansion speed as a function of redshift. So confident were they that the expansion had to decelerate due to gravitational interaction of galaxies that they introduced the so-called deceleration parameter q_0 , thought to be positive[1]. Together with H_0 , the deceleration parameter remained, for some time, the main cosmological parameters accessible to measurement. Nowadays, one prefers to describe the variation of the expansion of the universe in terms of the energy density of its constituents and their equation of state.

These first “classical tests” of the expansion involved measuring brightnesses of galaxies, but questions concerning galaxy brightness evolution with redshift rapidly surfaced and astronomers started looking for a better standard candle. The accelerated expansion was finally discovered at the very end of the last century and came as a surprise [2,3]. The two teams of discoverers

were aiming at measuring the matter density parameter through the distance-redshift relation of Type Ia supernovae, and faced a paradox: when they fitted a matter-dominated cosmology to their data, the matter density parameter had to be significantly negative. Relying on the reproducibility of Type Ia supernova explosion, the two projects were, by the end of the 1990, gaining access for the first time to a precise distance-redshift relation extending to $z \sim 0.7$ (about half of the age of the universe), and the observed relation favored an accelerated expansion. This was surprising because there is no room for an accelerated expansion in a matter-dominated universe. However, a cosmological model mixing matter and a cosmological constant could describe well these observations [2,3]. The cosmological constant enters in such a model as a source term with static density, while the matter density decreases with expansion.

Before the discovery of accelerated expansion, there had been earlier hints that matter might not constitute the dominant component of the universe at late times. In 1975, assuming that the brightest galaxy in galaxy clusters can be used as a standard candle (in a way very similar to type Ia supernovae), Gunn and Tinsley [4] boldly suggested that the universe was accelerating, but also (wrongly) concluded that the total energy density exceeds the critical density (the density for which the universe is spatially flat, see §2), and that deuterium cannot be formed in the early universe. In 1984, Peebles [5] gathered the arguments, mostly based on matter clustering (we discuss the physics at §2.2), in favour of a low matter density universe, and explicitly considered what has become our standard cosmological model. In 1990, the data from the new APM galaxy survey provided stronger evidence that the matter density is at most 1/3 of the critical density (see [6,7] and §5). And, in 1993, the measurement of the baryon fraction in galaxy clusters (i.e. the ratio of visible to total mass, see §7), associated to the baryon density from big bang nucleosynthesis¹ also challenged the matter-dominated flat universe model [10], favouring as well about 1/3 of the critical density in matter. These indications favouring a low matter density universe call for some other content, when associated to the theoretical prejudice of a flat (hence at critical density) universe². In this context, a low matter density calls for some sort of “complement”, although not necessarily causing acceleration. Note that observational evidence in favour of a critical matter-dominated universe was also produced concurrently (e.g. [11,12]). So, around 1997, observational cosmologists were mostly considering two possible models for the late-time universe:

¹ Big-Bang Nucleosynthesis (BBN) refers to the synthesis of nuclei via the fusion of light elements in the first minutes of the universe (see e.g. , §4 of [8] & [9]). The primordial abundance of light elements (and in particular He) depend on the baryon-to-photon density ratio then.

² Flatness is an inevitable consequence of the inflation theory, meant to solve some observation-based puzzles of hot big bang cosmology (see e.g. §8 of [8] and references therein).

a low matter density (sub-critical) universe, and a critical matter-dominated universe. Our current paradigm is both low matter density and flat. The discovery of accelerated expansion then reconciled the measurements of matter density with the theoretical inclination for a critical universe.

The accelerated expansion raises deep issues with likely connections to general relativity and particle physics. In the framework of general relativity a fluid with a static or almost static density may cause the acceleration of the expansion. The expression “dark energy” used nowadays refers to such a hypothetical fluid.

Although a cosmological constant still accurately describes all available large scale cosmological observations, phenomenologists have been studying a very vast range of possible models to incarnate dark energy. These models often involve scalar fields of some nature inspired by a range of particle physics or quantum gravity theories. We will not discuss these models here but refer to other papers of this special issue [13,14,15,16]. The distinguishing feature of these models (or at least of classes of model) is the way the density of dark energy evolves with the expansion, commonly described using the “equation of state” parameter w relating pressure and density $p = w\rho$. Non relativistic matter has $w = 0$, while a fluid of constant density (e. g. the cosmological constant) follows $w = -1$. We will report, in this review, on recent constraints obtained on w and discuss prospects for future improvements.

The discovery of an accelerated expansion was initially relying only on the distance-redshift relation of type Ia supernovae and the results were questioned. Could there be dust in the distant universe making distant supernovae appear dimmer? Were the supernovae brightnesses evolving with redshift? But independent observational evidence of an acceleration of the expansion grew rapidly. First, early ground based cosmic microwave background (CMB, discussed in §3) measurement pointing to a flat universe [17] which was hard to reconcile with observed low mass density without involving a non zero cosmological constant or something alike; then, the detection of the baryon acoustic oscillations (BAO, discussed in §5) in the galaxies two-point correlation function measured by the Sloan Digital Sky Survey [18]. We now have strong evidence for an accelerated expansion without invoking at all SNe Ia (e.g. §4.1 in [19], [20]), and, in a matter of a few years, a new model of the universe has emerged, the “concordance model”. In this model, the energy density content consists now of about a quarter of matter and three quarters of dark energy, often assumed to be of constant density, as observations indicate more and more tightly [21]. The cosmological model where dark energy is assumed to be the cosmological constant, Λ is called Λ CDM.

In this paper, we review the evidence for cosmic acceleration. In §2, we briefly describe the cosmological framework and introduce the observables for which

currents constraints are reported in §4 to 9, from observations obtained using a number of different techniques. An example of combined constraints on w and Ω_M is shown in §10. In §11, we briefly describe future projects that will help better constraint the acceleration and possibly shade new light on what could be the source of it. We conclude in §12.

This review is part of a 5 paper special issue on Dark Energy with the companion papers being: The Phenomenological Approach to Modeling Dark Energy[13], Everything You always Wanted to Know about the Cosmological Constant (but Were Afraid to Ask)[14], Establishing Homogeneity of the Universe in the Shadow of Dark Energy[15] and Galileons in the Sky[16].

2 Cosmic acceleration and dark energy

The cosmological principle states that the universe is homogeneous and isotropic, and the Friedman-Lemaitre-Robertson-Walker (FLRW) metric encodes this principle into its symmetries:

$$ds^2 = dt^2 - R^2(t) \left(\frac{dr^2}{1 - kr^2} + r^2(d\theta^2 + \sin^2 \theta d\phi^2) \right)$$

$R(t)$ is called the scale factor, and $k = -1, 0$ or 1 , is the sign of the spatial curvature³. Rather than $R(t)$, one often refers to $a(t) \equiv R(t)/T_{\text{now}}$. Objects with constant coordinates (r, θ, ϕ) are called comoving. In the FLRW framework, it is easy to show that photons emitted by comoving sources and detected by comoving observers see their wavelength scale with $R(t)$:

$$\frac{\lambda_{\text{reception}}}{\lambda_{\text{emission}}} = \frac{R(t_{\text{reception}})}{R(t_{\text{emission}})} \equiv 1 + z$$

where z is the redshift of the (comoving) source. General relativity postulates a relation between sources and the metric, which for the FLRW metric are called the Friedman equations [23]:

$$H^2(t) \equiv \left(\frac{\dot{R}}{R} \right)^2 = \frac{8\pi G}{3} \rho - \frac{k}{R^2(t)} + \Lambda/3 \quad (1)$$

$$\frac{\ddot{R}}{R} = -\frac{4\pi G}{3}(\rho + 3p) + \Lambda/3 \quad (2)$$

³ For textbooks covering these matters, we suggest [8,22].

where Λ is the cosmological constant, ρ stands for the energy density, and p for the pressure. The second equation is often called the Raychaudhuri equation. The energy conservation equation

$$\frac{d}{dt}(\rho R^3) = -3pR^2\dot{R} \quad (3)$$

relates pressure to density evolution and applies also separately to the various fluids in the universe. For non-relativistic matter, ρR^3 is constant and hence $p = 0$. A fluid with static density ($\dot{\rho} = 0$) has $p = -\rho$. In both Friedman equations, Λ could be summed into the density and pressure terms: $\rho_\Lambda = -p_\Lambda \equiv \Lambda/8\pi G$. Relation (3) can be obtained by eliminating \ddot{R} between Eq. 1 and 2.

Fluids can be characterised by a relation between p and ρ . The equation of state of each fluid w_X is defined by $p_X = w_X\rho_X$, and for a constant w_X , we have $\rho_X(t) \propto R(t)^{-3(1+w_X)}$. For matter $w = 0$, while $w = -1$ for Λ , and $w = 1/3$ for radiation. Given the densities at one epoch (e.g. now) and the equations of state of the fluids of the universe, one can solve the first Friedman equation (Eq. 1) for $R(t)$. One can define the current critical density i.e. the density for which $k = 0$, and the universe is flat:

$$\rho_c = \frac{3H_0^2}{8\pi G}$$

where $H_0 = (\dot{R}/R)_{now}$ is the Hubble constant. One conveniently expresses current densities in units of the current critical density:

$$\Omega_M = \frac{\rho_M}{\rho_c} = \frac{8\pi G\rho_M}{3H_0^2}, \quad \Omega_\Lambda = \frac{\Lambda}{3H_0^2}, \quad \Omega_k = -\frac{k}{R_0^2H_0^2}$$

and for, e.g., a universe of matter and a cosmological constant, the first Friedman equation simplifies to $1 = \Omega_M + \Omega_\Lambda + \Omega_k$. The quantity H_0 is often introduced into expressions under the form $h \equiv H_0/100\text{km/s/Mpc}$. For example, the matter physical density today is usually expressed as $\Omega_M h^2$, and turns out to be better determined than Ω_M .

From Eq. 2, one notes that a matter-dominated ($p \simeq 0$) universe or a radiation-dominated ($p > 0$) universe sees its expansion decelerate ($\ddot{R} < 0$). More generally, once one integrates Λ into density and pressure, the deceleration parameter $q(z)$ can then be expressed as:

$$q(z) \equiv -\frac{\ddot{R}}{RH^2} = \frac{1}{2} \sum_i \Omega_i(z) [1 + 3w_i(z)] \quad (4)$$

where $\Omega_i(z) \equiv \rho_i(z)/\rho_{\text{crit}}(z)$ is the fraction of critical density of component i at redshift z , and $w_i(z) \equiv p_i(z)/\rho_i(z)$, the equation of state of component i at redshift z . The sign of \ddot{R} is the one of the resulting $(\rho + 3p)$ ⁴. Therefore a fluid with $p < -\rho/3$ (i.e. $w < -1/3$) will cause the expansion to accelerate ($\ddot{R} > 0$) when it comes to dominate; its pressure is negative and pressure sources gravity in general relativity. By definition, such a component will be called dark energy. Note also that a mixture of matter and Λ (a $w = -1$ dark energy) sees its expansion accelerate as soon as $\rho_m < 2\rho_\Lambda$.

Following Frieman *et al* [24], we identify three possible classes of explanations for the acceleration of the expansion:

- (1) a source term in Friedman equations with a negative enough equation of state, for which various forms have been proposed from the simple vacuum energy Λ to more complicated time-variable scalar fields
- (2) Einstein equations of relativity need to be modified such as the acceleration is a manifestation of gravitational physics. This requires a modification of geometric part of the Einstein equation rather than of the stress-energy part ("left side as opposed to right side of the equations"). For this to work the modifications have to apply on large scales only.
- (3) A third explanation involves dropping the assumption that the universe is spatially homogeneous on large scales. The idea is that non linear gravitational effects of spatial density fluctuations should alter the distance-redshift relation (see below) in such a way that it would explain its apparent departure from a dark energy free universe.

It is not the purpose of this review to discuss the possible sources of acceleration. Here, we will rather concentrate on discussing the evidence for cosmic acceleration through constraints obtained the values of Ω_i and w_i as measured today. For an in-depth review of the phenomenology associated with the specific case of a cosmological constant, we refer the reader to [14].

The first constraints, which lead to the discovery of dark energy were obtained using type Ia supernovae to measure the distance-redshift relation

2.1 Cosmological distances and comoving volume

With the Friedman equation, one can integrate the photon path equation $ds = 0$ for $r(t)$, and compute various distances relevant to describe cosmological observations [25], as a function of redshift of the emitter and the parameters describing the source terms in the Friedman equation. For a source

⁴ In Newtonian gravity, since only masses source gravity, we would find ρ instead of $\rho + 3p$ there.

emitting a (rest frame) power L and with a measured energy flux F , the luminosity distance is defined by $d_L(z) \equiv \sqrt{L/4\pi F}$. Its expression as a function of cosmological parameters reads [25]:

$$d_L(z) = (1+z)H_0^{-1}|\Omega_k|^{-1/2}\text{Sin}\left\{|\Omega_k|^{1/2}r(z)\right\} \quad (5)$$

$$r(z) \equiv \int_0^z \frac{dz'}{H(z')} = \int_0^z [\Omega_M(1+z')^3 + \Omega_\Lambda + \Omega_k(1+z')^2]^{-1/2} dz'$$

where $\text{Sin}(x) = \sin(x), x, \sinh(x)$ for $k = 1, 0, -1$; note that the expression is continuous in $\Omega_k = 0$. This expression indicates that the distance-redshift relation probes the source terms of the Friedman equation. A Taylor expansion around $z = 0$ reads $d_L(z) = z/H_0 + O(z^2)$, which shows that densities only enter the expression beyond the first order in redshift. H_0 only enters as a global factor in the distance expression, so that $H_0 d_L$ only depends on redshift and reduced densities. One generalises Eq. 5 to alternatives to Λ (where dark energy might have a time-variable density) by replacing the Ω_Λ term by the (reduced) density of the considered fluid. For a constant equation of state, $\Omega_\Lambda \rightarrow \Omega_X(1+z)^{3(1+w)}$, and for a time-variable equation of state $w(z)$, $\Omega_\Lambda \rightarrow \Omega_X \exp[3 \int_0^z \frac{1+w(z')}{1+z'} dz']$. If one considers epochs when radiation was important, one should add $\Omega_r(1+z)^4$ to the sum of densities.

Fig. 1 displays the luminosity distance for a few cosmologies with varying admixtures of matter and cosmological constant, corresponding to a range of acceleration values now. One can note that the curve corresponding to our present Λ CDM paradigm cannot be mimicked with matter-dominated distance-redshift relations.

The angular distance d_A is defined via the apparent angular size θ of an object of comoving physical size D : $d_A \equiv D/\theta$. Because photons follow null-geodesics of the metric [26], we have $d_L = (1+z)^2 d_A$ and hence d_L and d_A convey the same cosmological information. d_L measurements rely on ‘‘standard candles’’ while d_A measurements rely on ‘‘standard rulers’’.

Comoving volumes can be used to constrain cosmological parameters from e.g. counts of objects of known comoving densities. For convenience, the comoving volume should be indexed by redshift :

$$\frac{d^2V}{dz d\Omega} = \frac{d_M^2(z)}{H(z)} \quad (6)$$

where $d_M = (1+z)d_A$.

2.2 Growth of structures

The expansion of the universe is accompanied by the increase in density contrast, essentially on all scales. This is called growth of structures. The subject is considerably more complex than homogeneous cosmologies and we will concentrate here on the salient features for what follows and point the interested readers to, e.g., chapter 15 of [22] (and references therein).

Density perturbations δ are defined by $1 + \delta(x) = \rho(x) / \langle \rho \rangle$. In the late universe, matter density perturbations follow the following differential equation:

$$\ddot{\delta} + 2H\dot{\delta} = 4\pi G\rho_M\delta. \quad (7)$$

where we have assumed that matter is pressure-less, radiation is negligible and we are considering scales (well) below the Hubble radius. This equation is perturbative in the sense that it results from a first order expansion, and requires in particular that $\delta \ll 1$. Dark energy impacts the growth of structures through its contribution to H and the evolution of $\rho_M(t)$. This equation has two solutions, and as a rule, at most one is growing. For a critical matter-dominated universe (an excellent approximation at $1000 > z > 1$), the growing mode follows $\delta(t) \propto a(t)$, which is called the ‘‘linear growth of structures’’. Fig. 2 displays the growth factor at late times of the growing solution for a set of chosen cosmologies.

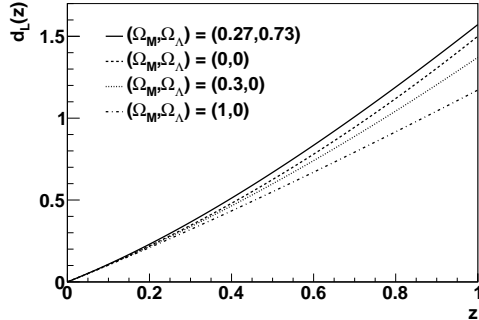


Fig. 1. *Luminosity distances for a few cosmologies ranging from now decelerating now to now accelerating. The Λ CDM cosmology (top curve) cannot be mimicked by any matter-dominated scenario.*

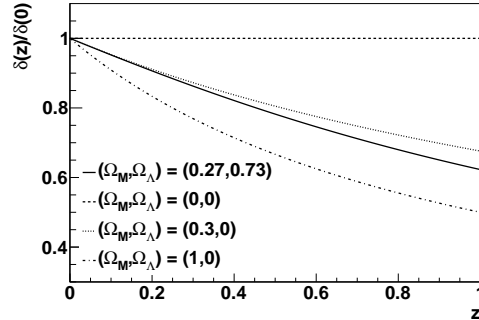


Fig. 2. *Linear growth factor (growing mode) for various cosmologies. Note that the ordering is quite different from distances of Fig. 1.*

In the early universe, matter perturbations still follow an equation similar to Eq. 7 with however two differences : the expansion rate is faster in a radiation-dominated universe, and when applicable, one should consider the couplings of radiation to charged matter, which allow sound waves to propagate in the

primordial plasma. In a radiation-dominated universe, matter density perturbations (both for charged and collision-free matter) grow logarithmically with time (i.e. very slowly), and hence, the horizon size, when matter and radiation densities are equal (the equality epoch), is imprinted in the matter power spectrum⁵. After equality, matter density perturbations grow, and the charged matter perturbations propagate as sound waves, until the temperature is small enough to allow atoms to form, at an epoch called “recombination”. The travel length of these sound waves is also imprinted in the matter correlation function as a (slight) excess at the comoving sound horizon size at recombination (see Fig. 3).

So, the clustering of matter contains two distinctive features: the horizon size at equivalence (which scales as $\rho_{M,0}^{-1}$) and the “sound horizon at recombination” (sometimes called the acoustic scale), which is a function of the matter and baryonic matter densities. Fig. 3 displays the canonical matter power spectrum and correlation function (they are related by a Fourier transform) at low redshift, where both features are visible.

2.3 Cosmic variance

Cosmological models do not predict the actual observed patterns, but rather their statistical properties, such as the average correlation function, or higher order statistics. Unavoidably, the comparison of observations with the model is limited by the ensemble variance of the observations, whatever their quality. This variance floor is referred to as “cosmic variance”, to be understood as cosmic sampling variance. For example, the theory predicts the average angular power spectrum of cosmic microwave background anisotropies (see §3), but we only observe a single map and cannot practically average over the observer location. The importance of cosmic variance in a given data set for measuring fluctuations at a given spatial scale can be appreciated in practice by evaluating the number of cells of this scale that the data set contains. The cosmic variance hence goes down when going to smaller spatial scales. The cosmic (sampling) variance has practical consequences: it sets a limit beyond which

⁵ Note that the electromagnetic radiation density is precisely known from FIRAS (aboard COBE) measurements [27] of Cosmic Microwave Background (CMB) temperature : $T_0 = 2.275 \pm 0.001K$ [28], and hence the CMB radiation density is known to $1.5 \cdot 10^{-3}$. This uncertainty has a negligible impact on our cosmological model [29]. Since neutrinos contribute to radiation density at equality, their number density relative to photons has to be assumed for the above arguments to hold. In particular, we *assume* that there are 3 neutrino species in the universe, i.e. that only the neutrinos with standard interactions (such as counted at the LEP collider) exist in the universe. CMB precision experiments now enter in a precision regime that might allow this hypothesis to be tested (e.g. [30]).

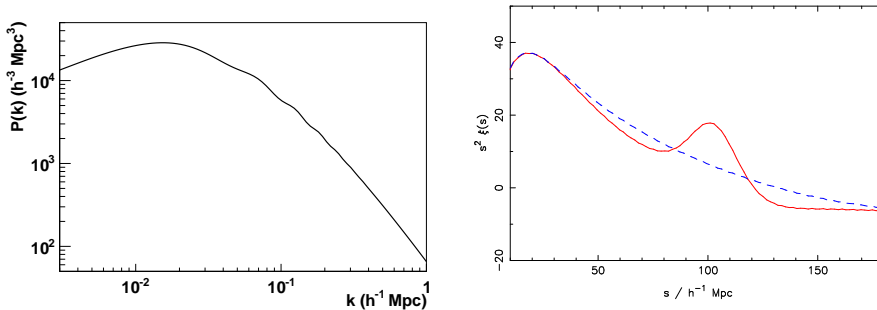


Fig. 3. *Left: dark matter power spectrum at $z=0$, computed using *CMBEasy* [31] for a flat standard Λ CDM, as a function of comoving wave number. The two key features are the maximum (which indicates the horizon size at matter-radiation equality, and depends on the matter density), and the series of wiggles which indicate the size of the sound horizon at recombination (and depends on matter and baryon densities). The latter corresponds to a single peak in direct space, as shown on the right. These features can be observed in Cosmic Microwave Background (CMB) anisotropies and galaxy redshift surveys, and their angular size constrains the expansion history. Right : the matter correlation function (times s^2) as a function of comoving separation s , for a universe without baryons (dashed line), or with baryons (full line). The acoustic peak (causing the wiggles in the power spectrum) is clearly visible (figure adapted from [32]).*

measuring more accurately the fluctuations will not improve significantly the cosmological constraints. For example, some surveys have mapped the three-dimensional positions of galaxies in some parts of the sky, up to a certain redshift, and the galaxy counts can be used as a proxy for the matter density field. Once the surveyed galaxy density is large enough for the Poisson noise to go below the cosmic variance, surveying the same volume by other means will not improve significantly our knowledge of e.g. the average power spectrum of the density field. Cosmic variance sets hard limits about the possible measurements of matter fluctuations on large scales in the nearby universe, and on the cosmic microwave background fluctuations on large angular scales. For the latter, the only practical approach consists in surveying the whole sky.

2.4 A brief survey of dark energy probes

Quantifying the merits of dark energy probes and predicting future dark energy constraints has been attempted by (at least) two working groups and the interested reader should consult their detailed reports [33,34]. Studying dark energy consists first in constraining its equation of state w , because the cosmological constant has $w = -1$ while other implementations give, in general, different values. This is constrained by measuring the expansion history, in practise the distance-redshift relation or more directly $H(z)$. The growth rate

of structures is another handle on dark energy, because it can deliver constraints on its own. More interestingly, measuring both the growth rate and the expansion history will allow us to test General Relativity on the largest spatial scales. All present evidence for dark energy rely on general relativity (more precisely the Friedman equations) properly describing gravitation on the largest spatial scales.

The expansion history is in practice constrained through the distance-redshift relation. Distances can be either luminosity distances from “standard candles”, or angular distances from “standard rods”. Today, the best known approximation to a standard candle is provided by type Ia supernovae, observable at redshifts beyond 1. For standard rods, baryon acoustic oscillations (BAO) provide the “acoustic peak” in the correlation function of matter, which requires large volume surveys to be detected, and we now have measurements over a few redshift bins. Standard rods measured across the line of sight constrain the angular distance and may directly constrain $H(z)$ when measured along the line of sight.

Gravitational lensing provides a handle on the matter distribution between distant galaxies and us. The “cosmic shear” phenomenon refers to weak lensing by large scale structures and allows one to constrain both distances and the matter clustering on large scales (and hence the growth of structures).

Studying the evolution of galaxy cluster counts with redshift allows one to constrain both the growth of structures (in a non-linear regime), and the expansion history through the comoving volume (Eq. 6).

Supernovae, baryon acoustic oscillations, weak lensing, and clusters were the four canonical dark energy probes studied at length in [33,34]. They remain today the main probes of cosmic acceleration. The next section is devoted to the particular role of CMB in dark energy constraints. The following sections then describe the principle behind the measurements and current achievements of each probe.

3 The role of the cosmic microwave background (CMB)

The cosmic microwave background (CMB) plays a particular role in constraining the acceleration of the expansion. Studying anisotropies (including polarisation) of CMB has become the key handle on cosmological parameters. The current best determination of cosmological parameters comes from seven years of observations with the WMAP satellite [35], and these results should be superseded by the Planck satellite in early 2013.

If dark energy density evolves slowly or not at all with redshift, it is negligible in the early universe, in particular before recombination, the epoch of CMB emission. However, dark energy impacts the angular scale of anisotropy correlations through our distance to the CMB emission (called last scattering surface or LSS), because dark energy contributes to the expansion rate at late times. Cosmological parameters hence contribute in two ways to the geometrical aspects of the observed anisotropies: directly in determining the detailed correlations of CMB anisotropies, and indirectly through our distance to LSS (see e.g. [36]). The physics of the acoustic waves is driven by the matter and baryon densities. Our distance to LSS depends on matter density, dark energy parameters, and the Hubble constant. At constant matter and baryon densities, and constant distance to LSS, the observed power spectrum of fluctuations is essentially unchanged (see e.g. [37]). CMB anisotropies thus provide a single constraint on dark energy and H_0 , which can be turned into a constraint on dark energy alone by using either a local measurement of H_0 , the flatness assumption (see e.g. [38] and references therein), or some other cosmological constraint. Assuming flatness and that dark energy is a cosmological constant, [35] obtains $\Omega_\Lambda = 0.727 \pm 0.030$. CMB constraints can of course be integrated into fits involving more general dark energy parameters, e.g. [21].

The CMB “geometrical degeneracy” is simply due to the fact that observations depend on a single distance: our distance to LSS. Secondary CMB anisotropies are the ones that build up as CMB travels to us, and hence break this degeneracy by introducing other distances. However, secondary anisotropies are subtle (e.g. [39]).

CMB is affected by the gravitational deflections of foreground structures: the image we obtain is remapped with respect to an homogeneous universe. This phenomenon has been studied in detail [40,41,42], and turns out to be a small correction to most of the observables. Recently a ground-based high resolution imager reported the detection of gravitational lensing of the CMB [43]. By introducing intermediate distances between us and LSS, the phenomenon breaks the geometrical degeneracy and allowed the same team to obtain a 3.2σ evidence for dark energy *from CMB alone* [44].

The integrated Sachs-Wolfe effect [45] is due to the time evolution of gravitational wells when photons traverse those, and the growth of structures is sensitive to dark energy. The Sachs-Wolfe effect only affects large scales, which are also the most affected by cosmic variance. Following a suggestion by [46], mild evidence for dark energy was found in [47] through the correlation of CMB temperature maps and galaxy distributions. Recent analyses [48,49] typically reach a 4σ detection of dark energy through this cross-correlation technique. Note that this detection is indeed independent of lifting the geometrical degeneracy of CMB.

Hence, the CMB *on its own* is of limited use when constraining dark energy. However since CMB constitutes the best probe to constrain our cosmological model (see e.g. [35]), its indirect contribution to dark energy constraints is essential (e.g. [50,51,21]). Most if not all recent studies forecasting dark energy constraints (see e.g. [33,34,52]) now assume they will eventually use “Planck priors” (e.g. [53]).

4 Hubble diagram of SNe Ia

Hubble originally published a distance-velocity diagram[54], which was the first indication of the expansion. We now call Hubble diagrams flux-redshift relations (or more commonly magnitude-redshift relations), for objects of similar intrinsic luminosity. Hubble initially reported distances to galaxies, but the chemical evolution of galaxies seems too fast to extend the galaxy “Hubble diagram” to high enough redshifts [55].

The Hubble diagram of type I supernovae was proposed to measure distances [56,57] and soon after to constrain the evolution of the expansion rate [58]. Supernovae are explosions of stars, and their taxonomy has been refined over the last 70 years. The current classification is detailed in e.g. [59,60]. Type Ia supernovae (SNe Ia) constitute an homogeneous subclass of supernovae, believed to be a complete thermonuclear combustion of a white dwarf reaching the Chandrasekhar mass ($1.4 M_{\odot}$), or the fusion of two white dwarfs (for a review of our current knowledge of progenitors, see [61]). These events are homogeneous in the sense that they show a reproducible luminosity (see e.g. [62]), and can hence be used to infer luminosity distances. The luminosity rises in about 20 rest frame days and fades over months (e.g. [63,64]) in visible bands. One usually uses the peak brightness as the primary distance indicator, which requires to measure the luminosity as a function of time (called “light curve”) in several spectral bands (see below). These events are bright enough to be measurable up to $z \simeq 1$ using ground-based 4-m class telescopes.

The Calan-Tololo survey delivered the first set of precise measurements of SNe Ia in 1996 [65], 29 events up to $z \sim 0.1$, which allowed the authors to get residuals to the Hubble diagram (magnitude-redshift) of 0.17 mag r.m.s or better⁶ (i.e. relative distance uncertainties of $\sim 8\%$). These distances make use of two empirical luminosity indicators, the decline rate of the light curves ([66,67]), and the color⁷ of the event (measured e.g. at peak luminosity).

⁶ Astronomical magnitudes are a logarithmic scale used to describe relative fluxes: $m = -2.5 \log_{10}(Flux/Flux_{ref})$

⁷ Colors are defined in astronomy as the ratio of fluxes measured in two different bands, or in practise the difference of magnitudes in two different bands. A typical

SNe Ia are sometimes called “standardisable candles”, and are the best known distance indicator to date.

In order to efficiently constrain cosmology from distances, one should use as long a redshift lever arm as possible: this is why cosmological constraints obtained from supernovae make use of nearby (typically $z < 0.1$) events, which, on their own, do not bring any interesting constraint on the expansion evolution. Those are however vital to almost all supernova cosmology analyses.

4.1 The discovery of the accelerated expansion

At the time the Calan-Tololo was succeeding at measuring distances, other teams were trying to discover and measure SNe Ia at $z \sim 0.5$, in order to probe the distance-redshift relation beyond the linear regime. Finding distant supernovae required using image subtraction techniques [68,69,70], which consist in digitally subtracting images of the same areas of the sky taken a few weeks apart in order to locate light excesses. These light excesses can then be spectroscopically identified (and their redshift measured), and eventually their light curves measured. Both methods and instruments for this demanding program started to be available at the beginning of the 1990’s, and by the end of the decade, the Supernova Cosmology project and the High-Z teams had collected large enough high redshift samples to start probing the cosmic acceleration. The two groups compared their high redshift ($z \sim 0.5$) sample to the Calan-Tololo nearby sample ($z < 0.1$) and reached the striking conclusion that no matter-dominated universe could describe their magnitude-redshift relation [2,3]. The measured high redshift distances are too large, compared to nearby ones, for a decelerating universe and all matter-only universes decelerate (see Eq. 2 and Fig. 1). All together the two projects had gathered ~ 50 distant events in total, and the shot noise affecting their photometry was significantly degrading the distance scatter compared to nearby events. A few years later, a sample of 11 events measured with the Hubble space telescope (HST), and featuring a photometric quality comparable to nearby events confirmed the picture [71].

Based on this success, second generation supernovae surveys were then launched, which aimed at constraining a constant equation of state of dark energy to 0.1 or better. This was carried out in two complementary ways: measuring distances to very high redshift supernovae using the HST, and running large dedicated ground-based surveys.

color indicator, widely used for distances to supernovae and elsewhere is B-V, where B is a (blue) filter covering [390,480]nm, and V covers the green region [500,600]nm.

4.2 *Second generation supernova surveys*

Very high redshift supernovae see their light shifted in the near IR, which is very difficult to observe from the ground because of the atmosphere large absorption bands, and emits a bright glow. Observing from space is then essentially mandatory for SNe Ia at $z > 1$. A large HST program was devoted to measuring distances to high redshift supernovae and delivered 37 events among which 18 were at $z > 1$ [72,73]. This sample extends deep enough in redshift to find evidence for a past deceleration era. Nowadays, the impact of this sample is however limited by the modest sampling of light curves and the photometric calibration uncertainties (discussed in e.g. §5.1.3 of [74]). More recently a higher quality sample of 10 HST $z > 1$ events was published [75], and confirms the picture.

Ground-based wide-field imagers can efficiently tackle the $z < 1$ regime by repeatedly imaging the same area of the sky, thus building light curves of variable objects. By tailoring the exposure time for a $z = 1$ supernova, a 1 deg² image delivers about 10 useful measurements of SN Ia light curves. The advent of wide-field imagers allowed observers to propose efficient second generation SN surveys relying on this multiplex advantage, with the promise of bringing new constraints on the equation of state of dark energy. Three surveys, which benefited from large observing time allocations, are listed here in the order of their median redshift:

- The SDSS SN search used the 1.4 deg² imager on the SDSS 2.5-m telescope to monitor 300 deg² in 5 bands every second night for 3 months a year during 3 years (2005-2007). The survey delivered light curves of ~ 500 spectroscopically identified SNe Ia to $z = 0.4$.
- The *Essence* project used the 0.36 deg² Mosaic-II imager on the CTIO-4m to monitor in 2 bands ~ 10 deg² for 3 months over 5 years (2003-2008), and has measured light curves of 228 identified SN Ia.
- The *SNLS* project relied on the 1 deg² Megacam imager on the 3.6-m Canada-France-Hawaii Telescope. It monitored 4 pointings in 4 bands for 5 years and measured the light curves of 450 spectroscopically identified SN Ia events to $z \sim 1$.

The three projects acquired as many spectra as they could to identify spectroscopically the candidates detected in the imaging program, and were limited by the amount of spectroscopic observing time. They however were able to increase the statistics of distant events by more than a factor 10, and these events have distance accuracies that compare well with nearby ones. During the last decade, second generation nearby SN surveys have also been run, and we now have about 120 high quality nearby events (see Tab 2. of [74]), and more to come.

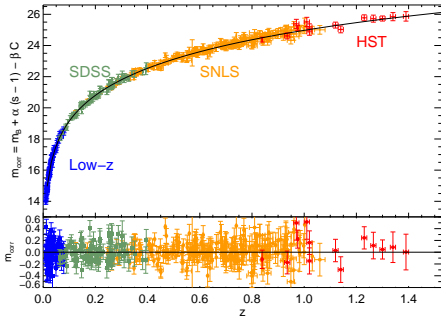


Fig. 4. *Recent Hubble diagram of SNe Ia (sample assembled in [74]). The largest samples are SNLS (3 years, [76]) and SDSS (1 year, [77]). The diagram contains about 500 events in total, and is compared to the best fit with supernovae only (Fig. from [21]).*

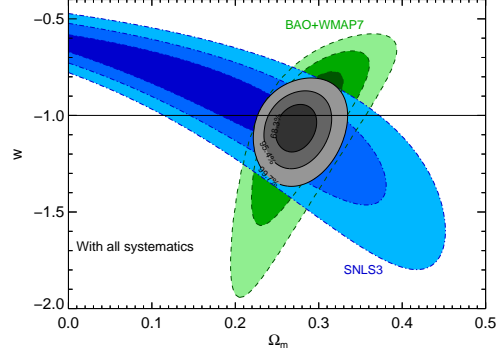


Fig. 5. *Cosmological constraints obtained from the Hubble diagram of Fig. 4 ([74]), from CMB anisotropies ([35]) and the matter power spectrum ([50]), and combined ([21]). The SN contours account for systematic uncertainties dominated by photometric calibration. Fig. from [21].*

So far, these 3 surveys have published partial analyses [78,79,77,74], and none has delivered its final sample yet. The latest compilation can be found in [74] which collects 3 years of SNLS, 1 year of SDSS, and the nearby samples, reaching a total of about 500 events passing stringent quality cuts, including spectroscopic identification. The resulting Hubble diagram is shown in Fig. 4. With a thorough accounting of systematic uncertainties, the cosmological fit of a flat universe where dark energy has a constant equation of state yields $w = -1.07 \pm 0.07$ [21] where the uncertainty accounts for both statistics and systematics, which contribute almost equally. This constraint, among the tightest to date, is illustrated on Fig. 5. It is highly compatible with the cosmological constant hypothesis.

5 Baryon acoustic oscillations (BAO)

The acoustic signatures observed in the CMB anisotropies survive recombination and leave their imprint on the matter distribution. Namely, the correlation function of matter density shows a peak at a comoving separation around 150 Mpc. This feature can be used as a standard ruler and can in principle be detected both along and across the line of sight, and yields constraints on $H(z)$ and the angular distance $d_A(z)$ respectively. Baryon acoustic oscillations are a small signal: the probability to find a galaxy pair at 150 Mpc separation is less than 1% larger than at 100 or 200 Mpc; detecting the signal require to survey at least a volume of the order of $1 h^{-3} Gpc^3$ (e.g. [80]).

So far, all detections made use of the galaxy distribution and merged the longitudinal and transverse directions. The first detections were reported in 2005 by the SDSS [18] and the 2dF [81] from the three-dimensional distribution of galaxies. Both surveys have made use of multi-object spectrographs, which allow one to collect hundreds of spectra at a time. Their samples of a few 100,000 galaxies used hundreds to thousands of observing nights. Both were redshift (i.e. 3 dimensional) galaxy surveys, limited to $z < 0.3$ for the 2dF and $0.16 < z < 0.47$ for the SDSS. The significance of BAO detections is modest (~ 2.5 to 3.5σ) but they add up since the samples map distinct volumes. Despite this modest significance, the SDSS measures the distance to the median redshift of the survey ($z = 0.35$) to better than 5% using the whole correlation function. Multi-band imaging data from the SDSS allows one to derive “photometric redshifts” of galaxies, and the volume thus covered extends to $0.2 < z < 0.6$ where the BAO signal is detected to 2.5σ [82]. Compared to spectroscopic redshifts, the noise of photometric redshifts blurs the BAO peak across the line of sight, and destroys the whole signal along the line of sight.

The SDSS spectroscopic sample has been doubled since the first detection[50], and the new WiggleZ survey has published its first results [32]; The measured correlation function is shown in Fig. 6. All these spectroscopic studies of BAO provide measurements of the acoustic scale at various redshifts and are usually expressed using a hybrid distance (proposed in [18]) :

$$D_V = \left[(1+z)^2 d_A^2(z) cz / H(z) \right]^{1/3} \quad (8)$$

which expresses that the measurement relies on two transverse and one longitudinal directions. The obtained constraints, independent of the acoustic scale and the growth of structure, are displayed in Fig. 6: they convey essentially the same information as the SN Hubble diagram, and reach very compatible conclusions, but are not as precise yet.

The redshifts surveys that deliver BAO constraints can also efficiently constrain the matter density from the shape of the matter power spectrum. In most of the analyses discussed above [81,18,50,32], a global fit to the matter correlation function or power spectrum yields essentially a constraint on Ω_M , which very efficiently complements distance measurements from SN to constrain dark energy.

The clustering of matter is sensitive to Ω_M , through the “horizon at equality” turnover discussed in § 2.2 and displayed in Fig. 3. Indeed, more than 20 years ago, one of the first measurements of the angular correlation of galaxies was found to be incompatible with an Einstein-De Sitter (flat $\Omega_M = 1$) universe[6,7], preferring $\Omega_M \simeq 0.3$, because this delays equality and shifts the turnover to larger spatial scales. With the prejudice of flatness, these results

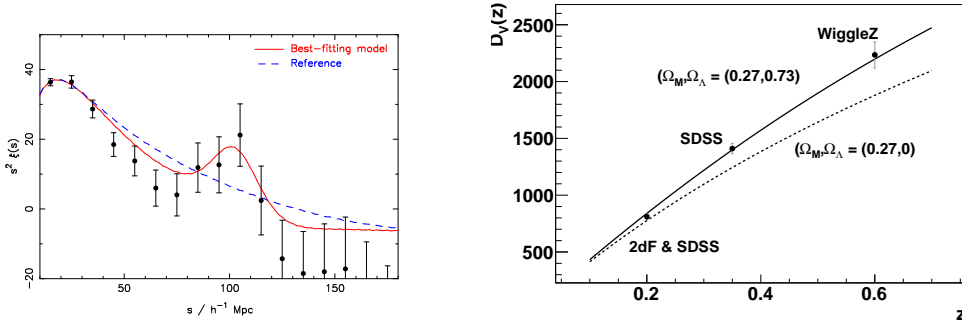


Fig. 6. *Right: correlation function from the WiggleZ redshift survey (borrowed from [32]) as a function of comoving separation, with the expectations from the best fitting model, and a baryon-free reference model. The acoustic peak is clearly visible, but note that the measured points are heavily correlated. Left: Distances measured in redshift slices from the acoustic feature in BAO surveys. The two low-redshift points come from [50] (which makes use of [81]), and the high redshift point is from [32]. The solid curve is the expectation for D_V (defined in Eq. 8), for a flat Λ CDM cosmology, where the overall scale was adjusted to the data. The dashed curve, does not much the data, even adjusting a global factor. In [83], a similar figure is proposed where the WiggleZ data is split into 3 overlapping (hence correlated) redshift bins.*

could be regarded as the first evidence for the presence of “something more than just matter”.

Cosmic variance really limits the reach of BAOs at low redshift: since the SDSS 2005 result [18] makes use of $\sim 10\%$ of the sky, is almost cosmic variance limited (sampling variance is about $1/3$ of cosmic variance), one should not expect more than a 10σ whole-sky detection of BAOs at $z < \sim 0.4$, at least using similar strategies. Similarly, cosmic variance limits the accuracy of a distance measurement to $z \sim 0.3$ using galaxy clustering over the whole sky to a few percent. This limitation rapidly vanishes as redshift rises, and is totally irrelevant at $z > 1$.

An interesting avenue for BAO surveys consists in accounting for the displacement of tracers with respect to their Hubble flow positions, due to their motions towards surrounding mass excesses. This technique, called “reconstruction”, was proposed [84], and applied on the SDSS data recently [85], where the variance of $D_V(z = 0.35)$ is remarkably improved by about a factor of 3. This technique is expected to be mostly effective in the low redshift universe, where it is very welcome because cosmic variance severely limits the ultimately achievable precision.

6 Direct measure of the growth rate

Three-dimensional galaxy redshift surveys allow one to probe the growth rate of fluctuations, assuming the expansion history is known. One relies on the distortion of redshift from velocity due to relative attraction of close-by galaxies which compresses their redshift difference[86]. Assuming one knows $d_A(z)$ and $H(z)$, and that galaxy clustering is isotropic on average, one can compare the clustering across and along the line of sight and detect these redshift distortions. For that, one defines the nuisance bias parameter b , assuming the relation

$$\left. \frac{\delta\rho}{\rho} \right|_{galaxies} = b \left. \frac{\delta\rho}{\rho} \right|_{mass}$$

and measurable e.g. by comparing the fluctuations of the CMB (evolved to current epoch using Eq. 7) with those of galaxy density, on spatial scales where perturbation theory holds. One thus measures a combination of parameters $\beta \equiv f/b$ ([86]), where $f \equiv d \log \delta / d \log R$ describes the growth rate, and approximately reads $\Omega_M^{0.6}$ for standard gravity in a wide class of cosmologies around Λ CDM (e.g. p. 378 of [8]).

The first evidence for redshift distortions were proposed in 2000 [87,88,89]. A more precise measurement from the two-degree-field galaxy redshift survey (2dfGRS) data (mostly at $z < 0.2$) [90] (using the amplitude of CMB fluctuations to derive bias) concludes that $\Omega_M \simeq 0.3$. Similar conclusions are reached using a smaller sample at $z \simeq 0.55$ [91].

Going to higher redshifts allows one in principle to probe the evolution of growth rate between then and now. In [92], the measurement at $z \sim 0.8$ is limited by the sample size of about 10,000 galaxies of the VIPERS survey, and measures the growth rate to 2.5σ . On a much larger volume, the WiggleZ survey measures the growth rate all the way to $z = 0.9$ at high significance [93] and discusses in detail the uncertainties in the way to account for non-linear effects, but does not venture into a fit of cosmological parameters.

To conclude, growth rate measurements from the redshift distortions are highly compatible with the current cosmological paradigm, not yet at a level to significantly contribute to cosmological constraints, and the way to overcome systematic uncertainties when measurements get more precise is still unclear. One may note that galaxy redshift surveys primarily aimed at measuring BAO over very large volume and redshift intervals will deliver high quality redshift distortion measurements in the same data sets.

7 Clusters of galaxies

The use of clusters of galaxies samples to study the acceleration of the universe started in the mid 1970's. At that time, brightest galaxies of clusters were used as standard candles to build Hubble diagrams extending to high enough redshifts that deviations from a straight Hubble line started to be detectable (see for example [94,95,96]). Interestingly, Gunn and Tinsley published in 1975 a letter titled "An accelerating Universe" (cautiously) reporting evidence that we live in an accelerating universe [4]. The conclusion was largely based on constraints obtained from measuring the brightness of galaxies in clusters [94].

These results, however, were marginally significant and possibly subject to large systematic errors as pointed by the authors themselves, in particular galaxy evolutionary corrections.

Most of the constraints derived from clusters nowadays are not obtained from a fit to a Hubble diagram but rather from the variation of the number density of clusters as a function of redshift as described below.

7.1 Clusters as cosmological probes

In the framework of the cold dark matter model, the number density of dark matter halos as a function of redshift can be calculated and compared to numbers obtained in large area cluster surveys that nowadays extend to high enough redshift.

Galaxy clusters are the largest virialized⁸ objects in the universe and are therefore expected to trace dark matter halos. The difficulty arises from the fact that clusters are, in practice, selected according to some observable O , such as X-ray luminosity or temperature. Other observables often used are cluster galaxy richness, weak lensing shear or Sunyaev-Zeldovich effect on the cosmic microwave background flux. The relation of these observable O selected cluster distributions with cluster mass distributions can be written as

$$\frac{d^2N(z)}{dzd\Omega} = \frac{d_M(z)}{H(z)} \int_0^\infty f(O, z) dO \int_0^\infty p(O|M, z) \frac{dn(z)}{dM} dM, \quad (9)$$

where $f(O, z)$ is the observable redshift dependent selection function, $dn(z)/dM$

⁸ In an expanding universe, strong over-densities no longer follow the expansion, and are bound. They approximately respect the virial relation between kinetic and potential energy, hence their name.

is the comoving density of dark halos, and $p(O|M, z)$ is the probability that a halo of mass M at redshift z is observed as a cluster with observable O .

Eq. (9) is sensitive to cosmology through the comoving volume element $d_M^2(z)/H(z)$ (Eq 6) and the growth of structure term, $dn(z)/dM$ which depends on the primordial spectrum and the evolution of density perturbations.

As mentioned above, several techniques are used to detect clusters as well as for estimating their masses. Systematic uncertainties, however, can greatly affect the determination of the mass-observable relation $p(O|M, z)$ and of the selection function $f(O, z)$ (see for example [97]).

Multi-band imaging, for example, allows clusters to be efficiently detected as excesses in the surface density of galaxies, and observed colors provide reliable enough redshift estimates that accidental projections can be greatly reduced. Moreover, various other effects such as weak lensing (e.g. [98]), can be used to calibrate the mass-observable relations. Although weak lensing seems a safe approach to evaluate cluster masses, unrelated large scale structures along the line of sight are a serious source of bias in this calibration, see e.g. [99,100].

Clusters are also detected in X-ray emitted by the hot baryon gas trapped in the dark matter potential well, and their mass derived from X-ray luminosity or gas temperature (see for example [101]).

Since it does not, in principle, depend on the source distance, the Sunyaev-Zeldovich effect can also be used to detect clusters out to higher redshift. (see for example [102]), and weak lensing can also provide cluster detections (e.g. [103]).

Another approach is to measure the baryonic gas mass from X-ray or SZ measurements and compare it with the virial mass estimates. The ratio of the two should be independent of redshift, which can only be achieved with the correct cosmology.

7.2 *Current cosmological constraints*

Cosmological constraints obtained from clusters have greatly improved during the last decade. X-ray observations of clusters obtained by “Chandra”, for example, have confirmed the acceleration of the expansion (see [105] and more recently [106]). Fig. 7 illustrates the power of cluster measurements to constraints acceleration. It shows that the measured mass function of clusters is correctly described provided a non zero amount of dark energy is accounted for in the model.

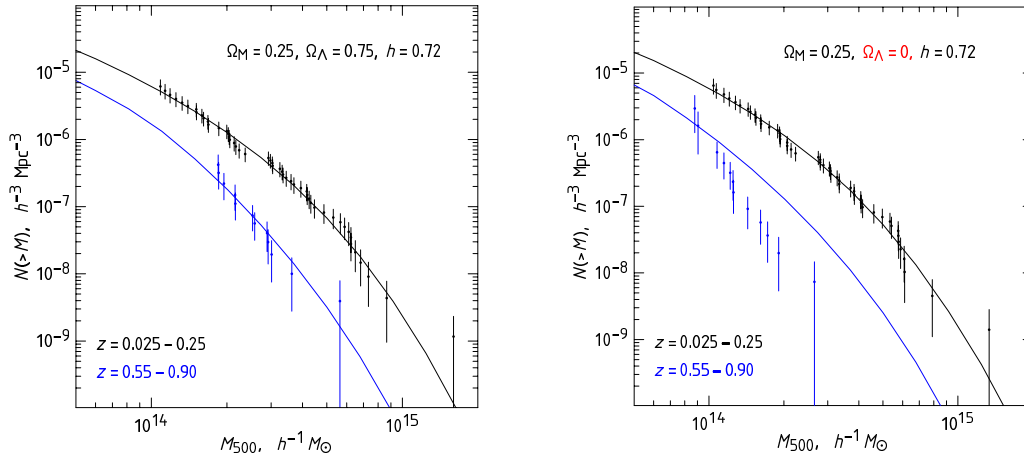


Fig. 7. Measured mass functions of clusters at low and high redshifts compared with predictions of a flat accelerating model and an open model without dark energy (from [104])

Taken as a whole, results obtained by most of the groups and using different techniques now agree at the $\sim 20\%$ precision level on the measurements of w and Ω_M (see Table 2 of [107]), and are in agreement with constraints obtained with other techniques. Clusters are now playing an important role in constraining the cosmic acceleration.

8 Gravitational lensing and cosmic shear

Gravitational lensing refers to the deflection of light by masses, or in a cosmological context by mass contrasts (see e.g. §2.4 of [22]). The transverse gravitational potential between sources and observers bends light bundles, thus remapping the image plane, which leaves observational signatures. Strong lensing refers to singular mappings, due to steep mass contrasts, and leads to spectacular signatures such as giant arcs and multiple images.

Weak lensing refers to non singular mappings and has tenuous observational signatures. The image displacement of distant galaxies is not observable but its gradient will coherently shear their images: locally, galaxies will display a coherent average elongation on top of natural randomly oriented ellipticities. This “cosmic shear” probes the density gradients, and the angular correlations of the cosmic shear probe the correlations of density perturbations (see e.g. [108,109,110]). The cosmic shear signal is weak : induced ellipticities are of order 0.01, when galaxies have natural ellipticities of ~ 0.3 [108], and one has to beat down this noise by brute force averaging. Shape distortions from the telescope (and atmosphere, when applicable) are commonly larger than the signal, and foreground stars are vital to map those distortions.

Rather than the mass power spectrum itself, its evolution with redshift (see Eq. 7) is sensitive to dark energy properties, and splitting the shear signal in source redshift slices improves cosmological constraints [111]. This technique called “lensing tomography”, is expected to deliver strong dark energy constraints in the future (e.g. [112]). For this application, redshift of galaxies can be approximate (however unbiased) and one uses “photometric redshifts” derived from multi-band photometry (considered for this purpose as coarse spectroscopy).

First evidence of cosmic shear were found in 2000 [113,114,115] from a few deg² surveys. In the following decade, two complementary paths were followed: improved galaxy shape measurements from the Hubble Space Telescope (HST), and much larger surveys from the ground. The COSMOS field covers 1.64 deg² imaged with the HST [116], which delivers an image quality (quantified by the size of star images) far better than from the ground. Multi-band photometry from UV to IR has been collected from ground and space to estimate the photometric redshifts. Using shear tomography, a $\sim 90\%$ CL evidence for acceleration was obtained from this data set [117].

The wide CFHT legacy survey (CFHTLS, 2003-2008) has collected images on 170 deg² in five bands from the ground. Preliminary results do not use the tomography ([118] and references therein), find a signal amplitude compatible with Λ CDM, measure the signal on large angular scales where perturbation theory applies, and detect the expected signal rise with redshift of sources. Shear tomography results from this survey are expected very soon (see cfhtlens.org), but given the survey area, dark energy constraints cannot yet outperform the current supernova and cluster counts results.

9 Age of the universe

Given a current cosmological model, one can integrate the Friedman equation and derive the time elapsed since the Big Bang. The uncertainties associated to the exact nature of the “beginning” are totally negligible in this context. In a matter-dominated universe, the age of the universe tends to $t_0 = H_0^{-1}$ for low matter density, reads $t_0 = 2/3H_0^{-1}$ for a flat universe, and has even shorter values for closed universes. For $H_0 = 70\text{km/s/Mpc}$, $H_0^{-1} \simeq 13$ Gy.

An observational lower limit on the age of the universe can be derived from the confrontation of star models with real stars. The constraint is cosmologically relevant since the oldest stars in globular clusters have an age $12 < t_0 < 15$ Gy [119]. For a matter-dominated universe, all densities but $\Omega_M \lesssim 0.1$ yield shorter ages, which is incompatible with constraints from galaxy clustering (§5). With dark energy, we can have both a ~ 13 Gy age and a low mat-

ter density ($\Omega_M \sim 0.3$) : cosmological models accelerating now had a slower expansion in the past and hence predict a larger age than the same models without dark energy.

The CMB anisotropies measure the distance to last scattering surface (LSS) (i.e. when hydrogen atoms combine and light no longer scatters), which is an increasing function of age. In a flat Λ CDM model, the CMB anisotropies constrain $t_0 = 13.77 \pm 0.13$ [35]. The constrain involves either the flatness assumption or some other measurement, such as a local H_0 measurement.

10 Current constraints on dark energy

Figure 8 displays a recent combination of constraints on a constant dark energy equation of state in a spatially flat universe (extracted from [107]). Overplotted are constraints obtained from WMAP [120], SNIa [121], BAO [122], abundance and growth of RASS clusters at $z < 0.5$ (labeled XLF; [105]) and gas fraction measurements at $z < 1.1$ [123], as well as the combined result shown by the orange (95%) and yellow (68%) confidence ellipses. Current precisions on these parameters are at the level of 10% both statistically and for systematics.

So far in this review, we have mainly discussed the achievements of observational programs in measuring the equation of state parameter w , assuming that w does not vary with cosmic time. w characterises the evolution with redshift of the dark energy density: for a constant w , $\rho_{DE} \propto (1+z)^{3(1+w)}$, and more generally, $\dot{\rho}_{DE} = -3\rho_{DE}H(1+w)$. When challenging the cosmological constant paradigm, or simply aiming at a finer characterisation of dark energy, one may consider a first order variation of the equation of state such as [124]: $w(z) \equiv w_0 + w_a(1-a) = w_0 + w_az/(1+z)$, where w_a characterises the variation. Since observations span at most $0 < a \leq 1$, only confidence intervals significantly smaller than 1 are really constraining. Unsurprisingly, this has not happened yet, even when fits gather essentially all available data: [35] reports $w_a = -0.38 \pm 0.66$ (flat universe), and with more supernovae but a careful accounting of systematic uncertainties [21] finds $w_a = -0.984 \pm 1.09$. So, the current limits on a varying equation of state are of limited interest. Future large projects such as Euclid, WFIRST or LSST could bring the uncertainty of w_a down to about 0.2 provided their level of systematics uncertainties are kept low.

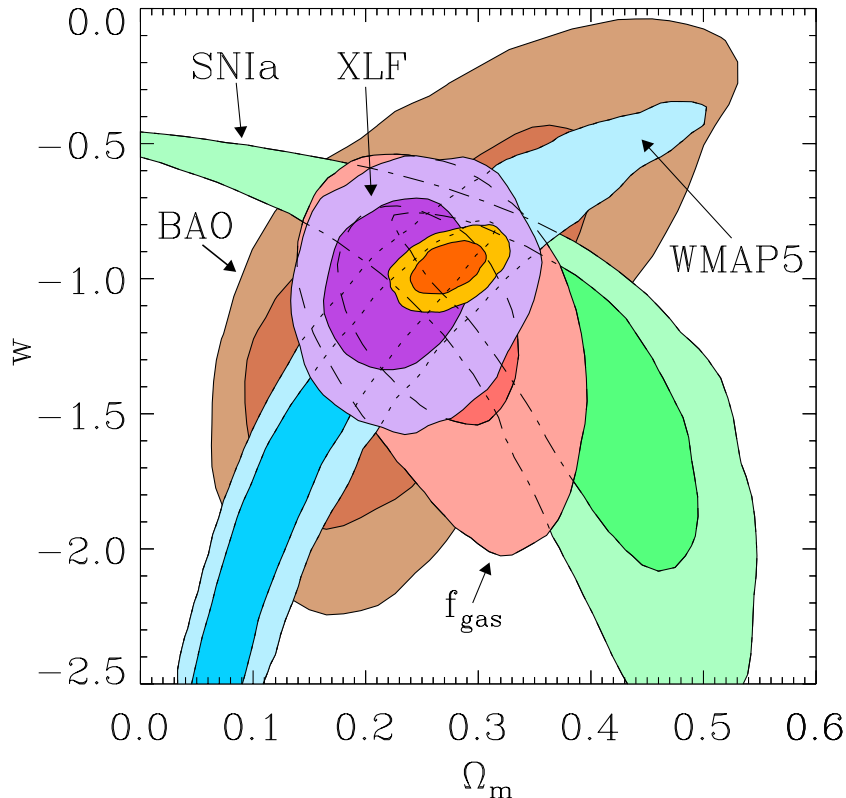


Fig. 8. *Joint 68.3% and 95.4% confidence regions for the dark energy equation of state and mean matter density (from [107])*

11 Future and prospects

Dark energy science relies today almost entirely on imaging and spectroscopy in the visible and near infrared. Several new wide-field imaging projects are starting to take data or soon will. The Table below summarizes the key figures of some present and future instruments and the size of anticipated (or executed) observing programs. Only currently approved programs are listed. They are imaging programs at the exception of the Euclid project, which will carry out both imaging and spectroscopy for high redshift galaxy survey. There are very few wide-field spectroscopy projects and Euclid's galaxy redshift survey is the main approved program in this field.

Regarding dark energy constraints these projects might deliver in the future, the main forecasts [33,34] show that systematic uncertainties are at play for all dark energy probes, and insist on a multi-probe approach. One should also note that all these telescopes will deliver data sets of major interest besides dark energy.

Second generation supernova surveys are expected to deliver their final samples in the next two years. This will amount to about 1000 distant events

Project	Mirror \varnothing (m)	Area (deg ²)	First light	Large survey (nights)
CFHT/Megacam	3.6	1.	2002	500
Pan-STARRS	1.8	7.	2009	>1000
Blanco/DEC	4.0	3.	2012	500
Subaru/HSC	8.2	1.8	2013	~500
LSST	6.5	10.	2019	3500
Euclid	1.2	0.5	2019	5 years

Table 1

Key figures for the major past and future wide-field imaging facilities. SNLS was part of the CFHTLS, a cosmology-oriented 500-night survey, executed at CFHT. Pan-STARRS, is currently constructing a second telescope and aims at eventually operating 4 of them. The 500-night survey to be run at the CTIO-Blanco is called Dark Energy Survey (DES). LSST main mirror diameter is 8.4 m but suffers from a 5 m central occultation. This facility will almost entirely observe in survey mode during its anticipated 10-year lifetime. Euclid is an approved ESA space project meant to observe in visible and near IR.

(at $z > 0.1$) and a growing set of nearby supernovae. Pan-STARSS is running a supernova program, DES is expected to [125], as well as LSST. Euclid does not currently have a supernovae program, although such a program could significantly contribute to dark energy constraints [126]. The accuracy of cosmological constrains will primarily depend on the accuracy of the relative photometric calibration of the various samples.

Although weak lensing has not delivered strong dark energy constraints yet, it concentrates hopes for the future: forecasts place the shear correlations ahead of all other dark energy probes (e.g. [33,34,52]). However, measuring the shear field from galaxy shapes is a difficult problem (see e.g. [127] and references therein), and relies on a very precise knowledge of the imaging system response (e.g. [128] and references therein). Current methodologies [129] are improving rapidly but still behind the required measurement accuracy [130]. One can now distinguish two observational complementary approaches: high signal to noise repeated measurements from the ground (pursued by LSST), and high resolution images from space (pursued by Euclid). Besides the difficult shear measurement, the comparison with expectations is not straightforward on small spatial scales, because of non linearity (e.g. [131]) and poorly known “baryon” physics [132]. The observations required for tomographic shear measurements also allow one to measure cosmic magnification statistics [133], which are free of all issues associated to shear measurements. Both approaches probe the same density field but with unrelated systematics, and can hence be compared without cosmic variance.

Galaxy redshift surveys have been dominated lately by WiggleZ and the SDSS. The SDSS telescope is currently running the BOSS program, to deliver galaxy redshifts up to $z \sim 0.7$, from which results are expected very soon (see [134]). Measuring BAO at large redshifts might come from the Fastsound redshift survey on Subaru, and also from the currently observing BOSS Quasar survey on SDSS-III [135]. Beyond these existing instruments, BigBOSS [136] constitutes a natural far-reaching ground-based follow-up project, but is not approved yet. Euclid's core program [52] includes a galaxy redshift survey (mainly at $z > \sim 0.8$) mostly for BAO and redshift distortions.

Over the next few years, the completion of the South Pole Telescope (SPT), the Atacama Cosmology telescope (ACT) and of the Planck SZ surveys will result in a large increase of the number of known clusters up to redshifts $z > 1$: about 1000 new clusters are expected to be discovered. Used in combination with existing optical and X-ray catalogs they should lead to significant improvement of our understanding of cluster growth and therefore further help constraint the acceleration of the expansion. However, calibration of mass proxies is likely to remain a limitation for these surveys and will require improvement of spatial resolution and sensitivity planned for the next generation of surveys such as the CCAT project. On the optical and near-infrared front, the large number of new ground-based surveys (see list above) will also result in a significant increase of the number of clusters and provide needed additional data such as the photometric redshifts and lensing data. Here again, the difficulty will be to define improved mass proxies in the redshift range of interest. In space, the planned Euclid and WFIRST near-infrared missions will allow cluster studies and measurements to be extended to higher redshifts and larger volumes to be probed. X-ray clusters samples detected with Chandra and XMM-Newton will help, in the near future, improve cosmological constraints from clusters. They will pave the way to the use of high statistics from the eROSITA X-ray telescope, which is expected to detect more than 50000 clusters with unprecedented purity and completeness.

12 Summary and conclusions

Thirteen years after its discovery the acceleration of the expansion is now firmly established and the concordance model constitutes the frame of a standard model of cosmology. Several techniques are now used at telescopes around the world to probe dark energy following, and sometimes driving, the fast development of wide-field imaging and multi-object spectroscopy, and making use of increased precision X-ray and CMB measurements. Of those techniques, SN and BAO are the most developed today, closely followed by the use of galaxy clusters, which has made considerable progress in the last few years and the emerging use of weak shear which promises to become one of the best tools to

measure dark energy. All these techniques make use of the impressive precision on cosmological parameters obtained by WMAP, soon to be improved by Planck results. One of the key features and power of using several techniques is that these techniques do not always probe the same domain of the cosmological model. Supernovae are a pure geometrical test, BAO are mostly geometrical too, while Weak Lensing and Clusters probe both geometry and growth of structure. Put together, they not only help break cosmological parameter degeneracies, but more importantly are subject to unrelated systematics. Mixing probes could also help finding out whether the acceleration of the expansion requires changing gravity on large scale or not.

To date, constraints on the dark energy equation of state require combining different techniques and are at the level of 10% both statistically and for systematics. In the future, with the coming next generation of experiments, each technique, combined with CMB precision measurements from the Planck satellite, will provide individual constraints on the dark energy equation of state, and combined they should be able to reach percent level precision. These projects may or may not see departure from $w = -1$ but if they do or if w is found to vary with time, they would rule out a cosmological constant or vacuum energy as the source of acceleration and open the way to new physics. Likewise, if the values of w determined from geometry or growth of structure methods are not equal, it would point toward a modification of gravity as the cause of acceleration. The next decade could bring important new observational clues on the origin of the acceleration of the expansion.

References

- [1] Sandage, A. The Ability of the 200-INCH Telescope to Discriminate Between Selected World Models. *ApJ*, 133:355–+, March 1961.
- [2] Riess, A. G., Filippenko, A. V., Challis, P., et al. Observational Evidence from Supernovae for an Accelerating Universe and a Cosmological Constant. *AJ*, 116:1009–1038, September 1998.
- [3] Perlmutter, S., Aldering, G., Goldhaber, G., et al. Measurements of Omega and Lambda from 42 High-Redshift Supernovae. *ApJ*, 517:565–586, June 1999.
- [4] Gunn, J. E. & Tinsley, B. M. An accelerating Universe. *Nature*, 257:454–457, October 1975.
- [5] Peebles, P. J. E. Tests of cosmological models constrained by inflation. *ApJ*, 284:439–444, September 1984.
- [6] Maddox, S. J., Efstathiou, G., Sutherland, W. J., & Loveday, J. Galaxy correlations on large scales. *MNRAS*, 242:43P–47P, January 1990.

- [7] Efstathiou, G., Sutherland, W. J., & Maddox, S. J. The cosmological constant and cold dark matter. *Nature*, 348:705–707, December 1990.
- [8] Kolb, E. W. & Turner, M. S. *The early universe*. (Front. Phys., Addison-Wesley), 1990.
- [9] Wagoner, R. V. Big-Bang Nucleosynthesis Revisited. *ApJ*, 179:343–360, January 1973.
- [10] White, S. D. M., Navarro, J. F., Evrard, A. E., & Frenk, C. S. The baryon content of galaxy clusters: a challenge to cosmological orthodoxy. *Nature*, 366:429–433, December 1993.
- [11] Loh, E. D. & Spillar, E. J. A measurement of the mass density of the universe. *ApJ*, 307:L1–L4, August 1986.
- [12] Nusser, A. & Dekel, A. Omega and the initial fluctuations from velocity and density fields. *ApJ*, 405:437–448, March 1993.
- [13] Kunz, M. *The Phenomenological Approach to Modeling Dark Energy*. 2012.
- [14] Martin, J. *Everything You always Wanted to Know about the Cosmological Constant (but Were Afraid to Ask)*. 2012.
- [15] Clarkson, C. *Establishing Homogeneity of the Universe in the Shadow of Dark Energy*. 2012.
- [16] de Rham, C. *Galileons in the Sky*. 2012.
- [17] de Bernardis, P., Ade, P. A. R., Bock, J. J., et al. A flat Universe from high-resolution maps of the cosmic microwave background radiation. *Nature*, 404:955–959, April 2000.
- [18] Eisenstein, D. J., Zehavi, I., Hogg, D. W., et al. Detection of the Baryon Acoustic Peak in the Large-Scale Correlation Function of SDSS Luminous Red Galaxies. *astro-ph/0501171*, January 2005.
- [19] Spergel, D. N., Bean, R., Doré, O., et al. Three-Year Wilkinson Microwave Anisotropy Probe (WMAP) Observations: Implications for Cosmology. *ApJS*, 170:377–408, June 2007.
- [20] Blanchard, A., Douspis, M., Rowan-Robinson, M., & Sarkar, S. Large-scale galaxy correlations as a test for dark energy. *A&A*, 449:925–928, April 2006.
- [21] Sullivan, M., Guy, J., Conley, A., et al. SNLS3: Constraints on Dark Energy Combining the Supernova Legacy Survey Three-year Data with Other Probes. *ApJ*, 737:102, August 2011.
- [22] Peacock, J. A. *Cosmological Physics*. (Cambridge University Press), 1999.
- [23] Friedmann, A. Über die möglichkeit einer welt mit konstanter negativer krümmung des raumes. *Zeitschrift für Physik A Hadrons and Nuclei*, 21:326–332, 1924. 10.1007/BF01328280.

- [24] Frieman, J. A., Turner, M. S., & Huterer, D. Dark Energy and the Accelerating Universe. *ARA&A*, 46:385–432, September 2008.
- [25] Carroll, S. M., Press, W. H., & Turner, E. L. The cosmological constant. *ARA&A*, 30:499–542, 1992.
- [26] Etherington, I. M. H. On the Definition of Distance in General Relativity. *Philosophical Magazine*, 15:761, 1933.
- [27] Mather, J. C., Cheng, E. S., Cottingham, D. A., et al. Measurement of the cosmic microwave background spectrum by the COBE FIRAS instrument. *ApJ*, 420:439–444, January 1994.
- [28] Fixsen, D. J. & Mather, J. C. The Spectral Results of the Far-Infrared Absolute Spectrophotometer Instrument on COBE. *ApJ*, 581:817–822, December 2002.
- [29] Hamann, J. & Wong, Y. Y. Y. The effects of cosmic microwave background (CMB) temperature uncertainties on cosmological parameter estimation. *J. Cosm. Astropart. P.*, 3:25, March 2008.
- [30] Keisler, R., Reichardt, C. L., Aird, K. A., et al. A Measurement of the Damping Tail of the Cosmic Microwave Background Power Spectrum with the South Pole Telescope. *ApJ*, 743:28, December 2011.
- [31] Doran, M. CMBEASY: an object oriented code for the cosmic microwave background. *J. Cosm. Astropart. P.*, 10:11, October 2005.
- [32] Blake, C., Kazin, E. A., Beutler, F., et al. The WiggleZ Dark Energy Survey: mapping the distance-redshift relation with baryon acoustic oscillations. *MNRAS*, pages 1598–+, October 2011.
- [33] Albrecht, A., Bernstein, G., Cahn, R., et al. Report of the Dark Energy Task Force. *ArXiv Astrophysics e-prints*, September 2006.
- [34] Peacock, J. A., Schneider, P., Efstathiou, G., et al. ESA-ESO Working Group on "Fundamental Cosmology". Technical report, October 2006.
- [35] Komatsu, E., Smith, K. M., Dunkley, J., et al. Seven-year Wilkinson Microwave Anisotropy Probe (WMAP) Observations: Cosmological Interpretation. *ApJS*, 192:18–+, February 2011.
- [36] Hu, W. Dark Energy Probes in Light of the CMB. In S. C. Wolff & T. R. Lauer, editor, *Observing Dark Energy*, volume 339 of *Astronomical Society of the Pacific Conference Series*, page 215, August 2005.
- [37] Bond, J. R., Efstathiou, G., & Tegmark, M. Forecasting cosmic parameter errors from microwave background anisotropy experiments. *MNRAS*, 291:L33–L41, November 1997.
- [38] Riess, A. G., Macri, L., Casertano, S., et al. A 3% Solution: Determination of the Hubble Constant with the Hubble Space Telescope and Wide Field Camera 3. *ApJ*, 730:119, April 2011.

- [39] Aghanim, N., Majumdar, S., & Silk, J. Secondary anisotropies of the CMB. *Reports on Progress in Physics*, 71(6):066902, June 2008.
- [40] Seljak, U. Gravitational Lensing Effect on Cosmic Microwave Background Anisotropies: A Power Spectrum Approach. *ApJ*, 463:1, May 1996.
- [41] Stompor, R. & Efstathiou, G. Gravitational lensing of cosmic microwave background anisotropies and cosmological parameter estimation. *MNRAS*, 302:735–747, February 1999.
- [42] Hu, W. Weak lensing of the CMB: A harmonic approach. *Phys. Rev. D*, 62(4):043007, August 2000.
- [43] Das, S., Sherwin, B. D., Aguirre, P., et al. Detection of the Power Spectrum of Cosmic Microwave Background Lensing by the Atacama Cosmology Telescope. *Physical Review Letters*, 107(2):021301, July 2011.
- [44] Sherwin, B. D., Dunkley, J., Das, S., et al. Evidence for Dark Energy from the Cosmic Microwave Background Alone Using the Atacama Cosmology Telescope Lensing Measurements. *Physical Review Letters*, 107(2):021302, July 2011.
- [45] Sachs, R. K. & Wolfe, A. M. Perturbations of a Cosmological Model and Angular Variations of the Microwave Background. *ApJ*, 147:73, January 1967.
- [46] Crittenden, R. G. & Turok, N. Doppler Peaks from Cosmic Texture. *Physical Review Letters*, 75:2642–2645, October 1995.
- [47] Scranton, R., Connolly, A. J., Nichol, R. C., et al. Physical Evidence for Dark Energy. *ArXiv Astrophysics e-prints*, July 2003.
- [48] Giannantonio, T., Scranton, R., Crittenden, R. G., et al. Combined analysis of the integrated Sachs-Wolfe effect and cosmological implications. *Phys. Rev. D*, 77(12):123520, June 2008.
- [49] Ho, S., Hirata, C., Padmanabhan, N., Seljak, U., & Bahcall, N. Correlation of CMB with large-scale structure. I. Integrated Sachs-Wolfe tomography and cosmological implications. *Phys. Rev. D*, 78(4):043519, August 2008.
- [50] Percival, W. J., Reid, B. A., Eisenstein, D. J., et al. Baryon acoustic oscillations in the Sloan Digital Sky Survey Data Release 7 galaxy sample. *MNRAS*, 401:2148–2168, February 2010.
- [51] Amanullah, R., Lidman, C., Rubin, D., et al. Spectra and Light Curves of Six Type Ia Supernovae at $0.511 < z < 1.12$ and the Union2 Compilation. *ArXiv e-prints*, April 2010.
- [52] Laureijs, R., Amiaux, J., Arduini, S., et al. Euclid Definition Study Report. *ArXiv e-prints*, October 2011.
- [53] Mukherjee, P., Kunz, M., Parkinson, D., & Wang, Y. Planck priors for dark energy surveys. *Phys. Rev. D*, 78(8):083529–+, October 2008.

- [54] Hubble, E. A Relation between Distance and Radial Velocity among Extra-Galactic Nebulae. *Proceedings of the National Academy of Science*, 15:168–173, March 1929.
- [55] Ostriker, J. P. & Tremaine, S. D. Another evolutionary correction to the luminosity of giant galaxies. *ApJ*, 202:L113–L117, December 1975.
- [56] Kowal, C. T. Absolute magnitudes of supernovae. *AJ*, 73:1021–1024, December 1968.
- [57] Kirshner, R. P. & Kwan, J. Distances to extragalactic supernovae. *ApJ*, 193:27–36, October 1974.
- [58] Wagoner, R. V. Determining q_0 from Supernovae. *ApJ*, 214:L5+, May 1977.
- [59] da Silva, L. A. L. The classification of supernovae. *Ap&SS*, 202:215–236, April 1993.
- [60] Filippenko, A. V. Optical Spectra of Supernovae. *ARA&A*, 35:309–355, 1997.
- [61] Howell, D. A. Type Ia supernovae as stellar endpoints and cosmological tools. *Nature Communications*, 2, June 2011.
- [62] Hamuy, M., Phillips, M. M., Suntzeff, N. B., et al. The Hubble Diagram of the Calan/Tololo Type IA Supernovae and the Value of H_0 . *AJ*, 112:2398–+, December 1996.
- [63] Leibundgut, B. *Light curves of supernovae type, I*. PhD thesis, PhD thesis. Univ. Basel.137 pp. , (1988), 1988.
- [64] Contreras, C., Hamuy, M., Phillips, M. M., et al. The Carnegie Supernova Project: First Photometry Data Release of Low-Redshift Type Ia Supernovae. *AJ*, 139:519–539, February 2010.
- [65] Hamuy, M., Phillips, M. M., Suntzeff, N. B., et al. BVRI Light Curves for 29 Type IA Supernovae. *AJ*, 112:2408–+, December 1996.
- [66] Pskovskii, Y. P. Photometric classification and basic parameters of type I supernovae. *Soviet Astronomy*, 28:658–+, December 1984.
- [67] Phillips, M. M. The absolute magnitudes of Type Ia supernovae. *ApJ*, 413:L105–L108, August 1993.
- [68] Hansen, L., Jorgensen, H. E., & Norgaard-Nielsen, H. U. Search for supernovae in distant clusters of galaxies. *The Messenger*, 47:46–49, March 1987.
- [69] Norgaard-Nielsen, H. U., Hansen, L., Jorgensen, H. E., Aragon Salamanca, A., & Ellis, R. S. The discovery of a type IA supernova at a redshift of 0.31. *Nature*, 339:523–525, June 1989.
- [70] Alard, C. & Lupton, R. H. A Method for Optimal Image Subtraction. *ApJ*, 503:325–+, August 1998.

- [71] Knop, R. A., Aldering, G., Amanullah, R., et al. New Constraints on Ω_M , Ω_Λ , and w from an Independent Set of 11 High-Redshift Supernovae Observed with the Hubble Space Telescope. *ApJ*, 598:102–137, November 2003.
- [72] Riess, A. G., Strolger, L., Tonry, J., et al. Type Ia Supernova Discoveries at $z < 1$ from the Hubble Space Telescope: Evidence for Past Deceleration and Constraints on Dark Energy Evolution. *ApJ*, 607:665–687, June 2004.
- [73] Riess, A. G., Strolger, L.-G., Casertano, S., et al. New Hubble Space Telescope Discoveries of Type Ia Supernovae at $z \geq 1$: Narrowing Constraints on the Early Behavior of Dark Energy. *ApJ*, 659:98–121, April 2007.
- [74] Conley, A., Guy, J., Sullivan, M., et al. Supernova Constraints and Systematic Uncertainties from the First Three Years of the Supernova Legacy Survey. *ApJS*, 192:1–+, January 2011.
- [75] Suzuki, N., Rubin, D., Lidman, C., et al. The Hubble Space Telescope Cluster Supernova Survey. V. Improving the Dark-energy Constraints above $z > 1$ and Building an Early-type-hosted Supernova Sample. *ApJ*, 746:85, February 2012.
- [76] Guy, J., Sullivan, M., Conley, A., et al. The Supernova Legacy Survey 3-year sample: Type Ia supernovae photometric distances and cosmological constraints. *A&A*, 523:A7+, November 2010.
- [77] Kessler, R., Becker, A. C., Cinabro, D., et al. First-Year Sloan Digital Sky Survey-II Supernova Results: Hubble Diagram and Cosmological Parameters. *ApJS*, 185:32–84, November 2009.
- [78] Astier, P., Guy, J., Regnault, N., et al. The Supernova Legacy Survey: measurement of Ω_M , Ω_Λ and w from the first year data set. *A&A*, 447:31–48, February 2006.
- [79] Wood-Vasey, W. M., Miknaitis, G., Stubbs, C. W., et al. Observational Constraints on the Nature of Dark Energy: First Cosmological Results from the ESSENCE Supernova Survey. *ApJ*, 666:694–715, September 2007.
- [80] Tegmark, M. Measuring Cosmological Parameters with Galaxy Surveys. *Physical Review Letters*, 79:3806–3809, November 1997.
- [81] Cole, S., Percival, W. J., Peacock, J. A., et al. The 2dF Galaxy Redshift Survey: power-spectrum analysis of the final data set and cosmological implications. *MNRAS*, 362:505–534, September 2005.
- [82] Padmanabhan, N., Schlegel, D. J., Seljak, U., et al. The clustering of luminous red galaxies in the Sloan Digital Sky Survey imaging data. *MNRAS*, 378:852–872, July 2007.
- [83] Blake, C., Kazin, E. A., Beutler, F., et al. The WiggleZ Dark Energy Survey: mapping the distance-redshift relation with baryon acoustic oscillations. *MNRAS*, 418:1707–1724, December 2011.

- [84] Eisenstein, D. J., Seo, H.-J., Sirko, E., & Spergel, D. N. Improving Cosmological Distance Measurements by Reconstruction of the Baryon Acoustic Peak. *ApJ*, 664:675–679, August 2007.
- [85] Padmanabhan, N., Xu, X., Eisenstein, D. J., et al. A 2% Distance to $z=0.35$ by Reconstructing Baryon Acoustic Oscillations - I : Methods and Application to the Sloan Digital Sky Survey. *ArXiv e-prints*, January 2012.
- [86] Kaiser, N. Clustering in real space and in redshift space. *MNRAS*, 227:1–21, July 1987.
- [87] Hamilton, A. J. S., Tegmark, M., & Padmanabhan, N. Linear redshift distortions and power in the IRAS Point Source Catalog Redshift Survey. *MNRAS*, 317:L23–L27, September 2000.
- [88] Taylor, A. N., Ballinger, W. E., Heavens, A. F., & Tadros, H. Application of Data Compression Methods to the Redshift-space distortions of the PSCz galaxy catalogue. *ArXiv Astrophysics e-prints*, July 2000.
- [89] Outram, P. J., Hoyle, F., & Shanks, T. The Durham/UKST Galaxy Redshift Survey - VII. Redshift-space distortions in the power spectrum. *MNRAS*, 321:497–501, March 2001.
- [90] Peacock, J. A., Cole, S., Norberg, P., et al. A measurement of the cosmological mass density from clustering in the 2dF Galaxy Redshift Survey. *Nature*, 410:169–173, March 2001.
- [91] Ross, N. P., da Ângela, J., Shanks, T., et al. The 2dF-SDSS LRG and QSO Survey: the LRG 2-point correlation function and redshift-space distortions. *MNRAS*, 381:573–588, October 2007.
- [92] Guzzo, L., Pierleoni, M., Meneux, B., et al. A test of the nature of cosmic acceleration using galaxy redshift distortions. *Nature*, 451:541–544, January 2008.
- [93] Blake, C., Brough, S., Colless, M., et al. The WiggleZ Dark Energy Survey: the growth rate of cosmic structure since redshift $z=0.9$. *MNRAS*, 415:2876–2891, August 2011.
- [94] Gunn, J. E. & Oke, J. B. Spectrophotometry of faint cluster galaxies and the Hubble diagram - an approach to cosmology. *ApJ*, 195:255–268, January 1975.
- [95] Kristian, J., Sandage, A., & Westphal, J. A. The extension of the Hubble diagram. II - New redshifts and photometry of very distant galaxy clusters - First indication of a deviation of the Hubble diagram from a straight line. *ApJ*, 221:383–394, April 1978.
- [96] Sandage, A., Kristian, J., & Westphal, J. A. The extension of the Hubble diagram. I. New redshifts and BVR photometry of remote cluster galaxies, and an improved richness correction. *ApJ*, 205:688–695, May 1976.

- [97] Henry, J. P., Evrard, A. E., Hoekstra, H., Babul, A., & Mahdavi, A. The X-Ray Cluster Normalization of the Matter Power Spectrum. *ApJ*, 691:1307–1321, February 2009.
- [98] Mandelbaum, R., Seljak, U., Baldauf, T., & Smith, R. E. Precision cluster mass determination from weak lensing. *MNRAS*, 405:2078–2102, July 2010.
- [99] White, M., van Waerbeke, L., & Mackey, J. Completeness in Weak-Lensing Searches for Clusters. *ApJ*, 575:640–649, August 2002.
- [100] Hoekstra, H., Hartlap, J., Hilbert, S., & van Uitert, E. Effects of distant large-scale structure on the precision of weak lensing mass measurements. *MNRAS*, 412:2095–2103, April 2011.
- [101] Arnaud, M., Pointecouteau, E., & Pratt, G. W. The structural and scaling properties of nearby galaxy clusters. II. The M-T relation. *A&A*, 441:893–903, October 2005.
- [102] Carlstrom, J. E., Holder, G. P., & Reese, E. D. Cosmology with the Sunyaev-Zel’dovich Effect. *ARA&A*, 40:643–680, 2002.
- [103] Miyazaki, S., Hamana, T., Ellis, R. S., et al. A Subaru Weak-Lensing Survey. I. Cluster Candidates and Spectroscopic Verification. *ApJ*, 669:714–728, November 2007.
- [104] Vikhlinin, A., Kravtsov, A. V., Burenin, R. A., et al. Chandra Cluster Cosmology Project III: Cosmological Parameter Constraints. *ApJ*, 692:1060–1074, February 2009.
- [105] Mantz, A., Allen, S. W., Rapetti, D., & Ebeling, H. The observed growth of massive galaxy clusters - I. Statistical methods and cosmological constraints. *MNRAS*, 406:1759–1772, August 2010.
- [106] Burenin, R. A. & Vikhlinin, A. A. Cosmological parameters constraints from galaxy cluster mass function measurements in combination with other cosmological data. *ArXiv e-prints*, February 2012.
- [107] Allen, S. W., Evrard, A. E., & Mantz, A. B. Cosmological Parameters from Observations of Galaxy Clusters. *ARA&A*, 49:409–470, September 2011.
- [108] Mellier, Y. Probing the Universe with Weak Lensing. *ARA&A*, 37:127–189, 1999.
- [109] Bartelmann, M. & Schneider, P. Weak gravitational lensing. *Phys. Rep.*, 340:291–472, January 2001.
- [110] Refregier, A. Weak Gravitational Lensing by Large-Scale Structure. *ARA&A*, 41:645–668, 2003.
- [111] Hu, W. Power Spectrum Tomography with Weak Lensing. *ApJ*, 522:L21–L24, September 1999.
- [112] Amara, A. & Réfrégier, A. Optimal surveys for weak-lensing tomography. *MNRAS*, 381:1018–1026, November 2007.

- [113] Van Waerbeke, L., Mellier, Y., Erben, T., et al. Detection of correlated galaxy ellipticities from CFHT data: first evidence for gravitational lensing by large-scale structures. *A&A*, 358:30–44, June 2000.
- [114] Bacon, D. J., Refregier, A. R., & Ellis, R. S. Detection of weak gravitational lensing by large-scale structure. *MNRAS*, 318:625–640, October 2000.
- [115] Wittman, D. M., Tyson, J. A., Kirkman, D., Dell’Antonio, I., & Bernstein, G. Detection of weak gravitational lensing distortions of distant galaxies by cosmic dark matter at large scales. *Nature*, 405:143–148, May 2000.
- [116] Scoville, N., Abraham, R. G., Aussel, H., et al. COSMOS: Hubble Space Telescope Observations. *ApJS*, 172:38–45, September 2007.
- [117] Schrabback, T., Hartlap, J., Joachimi, B., et al. Evidence of the accelerated expansion of the Universe from weak lensing tomography with COSMOS. *A&A*, 516:A63, June 2010.
- [118] Fu, L., Semboloni, E., Hoekstra, H., et al. Very weak lensing in the CFHTLS wide: cosmology from cosmic shear in the linear regime. *A&A*, 479:9–25, February 2008.
- [119] Krauss, L. M. & Chaboyer, B. Age Estimates of Globular Clusters in the Milky Way: Constraints on Cosmology. *Science*, 299:65–70, January 2003.
- [120] Dunkley, J., Komatsu, E., Nolta, M. R., et al. Five-Year Wilkinson Microwave Anisotropy Probe Observations: Likelihoods and Parameters from the WMAP Data. *ApJS*, 180:306–329, February 2009.
- [121] Kowalski, M., Rubin, D., Aldering, G., et al. Improved Cosmological Constraints from New, Old, and Combined Supernova Data Sets. *ApJ*, 686:749–778, October 2008.
- [122] Percival, W. J., Reid, B. A., Eisenstein, D. J., et al. Baryon acoustic oscillations in the Sloan Digital Sky Survey Data Release 7 galaxy sample. *MNRAS*, 401:2148–2168, February 2010.
- [123] Allen, S. W., Rapetti, D. A., Schmidt, R. W., et al. Improved constraints on dark energy from Chandra X-ray observations of the largest relaxed galaxy clusters. *MNRAS*, 383:879–896, January 2008.
- [124] Chevallier, M. & Polarski, D. Accelerating Universes with Scaling Dark Matter. *International Journal of Modern Physics D*, 10:213–223, 2001.
- [125] Bernstein, J. P., Kessler, R., Kuhlmann, S., et al. Supernova Simulations and Strategies For the Dark Energy Survey. *ArXiv e-prints*, November 2011.
- [126] Astier, P., Guy, J., Pain, R., & Balland, C. Dark energy constraints from a space-based supernova survey. *A&A*, 525:A7, January 2011.
- [127] Zhang, J. & Komatsu, E. Cosmic shears should not be measured in conventional ways. *MNRAS*, 414:1047–1058, June 2011.

- [128] Paulin-Henriksson, S., Refregier, A., & Amara, A. Optimal point spread function modeling for weak lensing: complexity and sparsity. *A&A*, 500:647–655, June 2009.
- [129] Bridle, S., Balan, S. T., Bethge, M., et al. Results of the GREAT08 Challenge: An image analysis competition for cosmological lensing. *ArXiv e-prints*, August 2009.
- [130] Amara, A. & Réfrégier, A. Systematic bias in cosmic shear: extending the Fisher matrix. *MNRAS*, 391:228–236, November 2008.
- [131] Sato, M., Hamana, T., Takahashi, R., et al. Simulations of Wide-Field Weak Lensing Surveys. I. Basic Statistics and Non-Gaussian Effects. *ApJ*, 701:945–954, August 2009.
- [132] Semboloni, E., Hoekstra, H., Schaye, J., van Daalen, M. P., & McCarthy, I. G. Quantifying the effect of baryon physics on weak lensing tomography. *MNRAS*, 417:2020–2035, November 2011.
- [133] van Waerbeke, L. Shear and magnification: cosmic complementarity. *MNRAS*, 401:2093–2100, January 2010.
- [134] Anderson, L., Aubourg, E., Bailey, S., et al. The clustering of galaxies in the SDSS-III Baryon Oscillation Spectroscopic Survey: Baryon Acoustic Oscillations in the Data Release 9 Spectroscopic Galaxy Sample. *ArXiv e-prints*, March 2012.
- [135] Le Goff, J. M., Magneville, C., Rollinde, E., et al. Simulations of BAO reconstruction with a quasar Ly- α survey. *A&A*, 534:A135, October 2011.
- [136] Schlegel, D., Abdalla, F., Abraham, T., et al. The BigBOSS Experiment. *ArXiv e-prints*, June 2011.